Journal of Catalysis 322 (2015) 60–72

Contents lists available at ScienceDirect

Journal of Catalysis

journal homepage: www.elsevier.com/locate/jcat

Oxalic acid at the TiO_2/water interface under UV(A) illumination: Surface reaction mechanisms ☆

Cecilia B. Mendive [a,b,*], Thomas Bredow [c], Jenny Schneider [b], Miguel Blesa [d], Detlef Bahnemann [b,e]

[a] Departamento de Química, Facultad de Ciencias Exactas y Naturales, Universidad Nacional de Mar del Plata, Dean Funes 3350, B7600AYL, Mar del Plata, Argentina
[b] Institut für Technische Chemie, Leibniz Universität Hannover, Callinstr. 3, D-30167 Hannover, Germany
[c] Mulliken Center for Theoretical Chemistry, Institut für Physikalische und Theoretische Chemie, Universität Bonn, Beringstraße 4, D-53115 Bonn, Germany
[d] Postgraduate School, Universidad Nacional de General San Martín, Peatonal Belgrano 3563, 1° piso, B1650ANQ, San Martín, Buenos Aires, Argentina
[e] Laboratory for Nanocomposite Materials, Department of Photonics, Faculty of Physics, Saint-Petersburg State University, Ulianovskaia str. 3, Peterhof, Saint-Petersburg, 198504, Russia

ARTICLE INFO

Article history:
Received 22 August 2014
Revised 18 November 2014
Accepted 20 November 2014

Keywords:
Photocatalysis
Titanium dioxide
Oxalic acid
Surface complexes
Surface reactions

ABSTRACT

It is through the comparison of experimental results and theoretical calculations that the mechanistic details of several surface photoreactions initiated upon UV(A) illumination of adsorbed oxalic acid on rutile and anatase can be proposed. The absorption of light is found to be rather localized at surface Ti atoms and at the adsorbed species on both TiO_2 polymorphs, respectively. Different surface complexes exhibit different photoreactivities, and consequently, each of them may follow a different reaction mechanism. Experimental data can be explained involving reactions such as the interconversion of monodentate into bidentate species which may further be oxidized to CO_2 or may even produce ·OH radicals, while the reduction of monodentate species to the respective aldehyde results in combination with the oxidation of a neighbouring adsorbed OH group into the formation of an adsorbed ·OOH radical. On the basis of the results presented herein, it is concluded that the direct action of the photocatalytically produced electron–hole pairs on the adsorbed species is the primary step of the photocatalytic reaction, while the intermediate formation of free radical species followed by their reaction with an oxalate molecule can be regarded as a secondary process. Within the system described in this work, ·OH radicals only appear to be produced following the direct interaction of a hole with the adsorbed organic compound, but not with chemisorbed water molecules.

1. Introduction

Considerable efforts have been spent on the development of TiO_2-based photocatalysts during the last 40 years [3] with the respective approaches ranging from fundamental research using model compounds to the large-scale fully technologically oriented development of environmental, disinfecting or energy applications. In most of the modern applications, TiO_2 is employed in the form of nanoparticles, thus enabling the utilization of the largest possible surface area. In these cases, particle size measurements should be regarded as a necessary prerequisite for their characterization, not only to compare the performance of different photocatalysts, but also as an essential tool for the investigation of their (photo)electronic properties [4–6]. In particular, when working with nanoparticles, the detailed knowledge of the nature of the exposed facets and of the atomic structure of the nanoparticles is of utmost interest due to their key role in the photocatalytic reaction mechanism [7,8]. Since, in particular, commercially produced TiO_2 nanocrystallites do not exhibit the equilibrium faces naturally occurring in macroscopic single crystals [9], photocatalytic reaction models assuming the well-known crystallographic facets may be unrealistic. Different exposed surfaces will definitively lead to different chemical interactions with a given adsorbate [1,2] due to a different coordination of the surface atoms, thus likely triggering different reaction mechanisms. A thorough study of the adsorption of oxalic acid at supported rutile [1] and anatase [2] nanoparticles showed the coexistence of different binding structures, resulting in different adsorption enthalpies. While at rutile (110) [1], the most stable and abundant structure is a bidentate complex, a monodentate structure is found to be the most favoured adsorbed oxalate species at the (100) anatase surface [2].

☆ This article is the third part (Part III) of a series of studies focused on the adsorption and photoreaction mechanisms of oxalic acid at nanoparticulate rutile and anatase. Parts I and II are references 1 and 2, respectively.

* Corresponding author at: Departamento de Química, Facultad de Ciencias Exactas y Naturales, Universidad Nacional de Mar del Plata, Dean Funes 3350, B7600AYL, Mar del Plata, Argentina.
E-mail address: cbmendive@mdp.edu.ar (C.B. Mendive).

http://dx.doi.org/10.1016/j.jcat.2014.11.008
0021-9517/

In the literature, there has been a general consensus concerning a higher photocatalytic activity of anatase as compared to rutile [10,11]. This picture was, however, likely biased by the technical difficulties in producing both, nanoparticulate rutile and anatase single crystals. Following tremendous advances in the respective synthetic procedures, rutile nanoparticles can nowadays be rather easily obtained in large quantities [12] thus enabling the exploration of their photocatalytic properties and fair comparisons with that of anatase [13]. The respective results yielded surprisingly similar photocatalytic activities for both polymorphs of comparative particle size [14]. And even though considerable efforts have been undertaken to unravel the mechanisms governing the surface reactions following the initial photocatalytic process, i.e. the electron–hole formation within the semiconductor nanoparticle [15], a large number of unanswered questions still exists the answers of which will most likely result in more accurate and reliable models. The description of the photocatalytic reaction pathways is usually simplified solely focusing on the chemical reactions of the adsorbed species, i.e. the individual molecules, neglecting any distinct participation of surface atoms as 'true species'. Furthermore, atoms belonging to the photocatalyst surface are usually described as a simple source of oxidizing (or reducing) entities, e.g. photogenerated holes formed upon UV(A) illumination are transformed at surficial oxygen atoms into surface bound hydroxyl radicals [16,17]. In general, investigations concerning reaction mechanisms involving the photocatalytic activity of TiO_2 at which the reactants are adsorbed are rather scarce [18–20].

Our respective studies have initially been focused on the role of surface complexes for the photocatalytic activity of aqueous TiO_2 systems [21] employing the widely used Evonik-Degussa Aerosil TiO_2 P-25 and oxalic acid as the model compound. For these studies, the structure of the adsorbed species was deduced from IR measurements, and the intriguing result was that the photocatalytic activity substantially differed for each of the different surface complexes [21]. Thus, it became apparent that a more precise knowledge of the nature and the structure of these surface complexes is required, resulting in a description of the system by means of a combination of experimental results and theoretical calculations [22]. Based upon these studies, a simplified and still rather qualitative mechanism was suggested for the photocatalytically induced reactions of adsorbed oxalate occurring at the surface of rutile (1 1 0) and anatase (1 0 0).

There are numerous theoretical studies concerning the adsorption of small and medium-sized molecules on low-index surfaces of TiO_2 (see, e.g. a review by Diebold [23] and further Refs. [24–30]). Most of them have been performed resembling a surface-science approach and are therefore suitable for a comparison with experiments performed under ultrahigh vacuum (UHV) conditions, but not for nanoparticles in solution. From the theoretical point of view, photochemical properties are often discussed in terms of Kohn–Sham orbital energies [31] instead of *n*-electron state energies explicitly including electron correlations. The importance of the solvent molecules on the surface and of the bulk properties of small TiO_2 particles has been taken into account only in a few studies [32,33].

Herein, we present the results of an *in situ* study of UV(A) irradiated rutile and anatase in contact with aqueous oxalic acid. Particular attention has been focussed on the characteristic adsorption structures at each crystalline phase as well as on the exploration of their time evolution under UV(A) illumination. This work aimed to identify the involved excited states aiming to suggest reaction mechanisms occurring directly at the surface of the TiO_2 nanoparticles. Thus, we were able to show that TiO_2 surface atoms play an active role in the photocatalytic reactions. A combination of theoretical calculations at the configuration interaction (CI) level and experimental results using attenuated total reflection Fourier-transformed infrared (ATR-FTIR) spectroscopy was thus employed to study the kinetics of the photocatalytic conversion of the involved surface complexes. However, the present investigation only represents a first step towards a sound understanding of the photodegradation mechanism of oxalic acid at illuminated titania surfaces. The suggested mechanisms are rather intended to provide the basis for future discussions as well as for more advanced investigations to be carried out by us or by other groups working in this field.

2. Experimental procedures

The same photocatalyst materials used previously for the respective experiments carried out under dark conditions [1,2] were employed in the present work. They consist of pure rutile (R15 provided by Millennium Inorganic Chemicals, now CRISTAL GLOBAL) and pure anatase (commercial product S230 from Kemira) nanoparticles with respective surface areas of 65 and 230 $m^2\ g^{-1}$ (BET adsorption) and average particle sizes of 15 nm (rutile) and 4–7 nm (anatase), respectively. Detailed information concerning these TiO_2 materials can be found in Refs. [1,2].

All ATR-FTIR *in situ* spectra were recorded on a BOMEM MB 122 instrument which was equipped with a liquid N_2-cooled MTC-A detector and a Pike Technologies horizontal ATR unit with a ZnSe crystal of 45° and 9 reflections in the upper face. Other reagents used in this work were of analytical grade and used as received. Deionized water from a SARTORIUS ARIUM 611 apparatus (conductivity = 0.182 $\mu S\ m^{-1}$) was employed for the preparation of the solutions and suspensions.

The UV(A) illumination source consisted of two tubes (PHILIPS CLEO 15 W), with a maximum emission at wavelengths between 300 and 400 nm placed directly above the ATR unit. The distance to the lamp from the ATR crystal was adjusted to provide 0.6 mW cm^{-2} at its surface. Details of the construction of the illumination set-up can be found in Ref. [22].

A TiO_2 (rutile or anatase) layer was deposited on the ZnSe ATR crystal (2.3 g m^{-2} and 1–3 μm thick) [1,2,22] by drying at room temperature an aliquot of 200 μl of a 5.75 g l^{-1} TiO_2 suspension together with 200 μl of water (see Refs. [1,2]). Prior to the production of the TiO_2 thin layer, the ATR prism surface was cleaned by polishing with 1 μm diamond paste (Metadi II, polishing grade) and rinsed with methanol and deionised water. This cleaning procedure was carried out under an optical microscope and with extreme care in order to ensure no damages to the ZnSe surface. Thus, identical initial conditions for every experiment were always restored since the formation of a precipitate on the ZnSe crystal was detected after long UV(A) irradiation times. Several tests were performed repeating two identical experiments and employing the ZnSe crystal containing the precipitate in one of them. These tests showed reproducible results evincing that the precipitate only acted as an attenuation filter diminishing the output signal to the detector, and was photochemically and chemically inert for the system. The nature of the precipitate was presumed to be metallic Se which could only be removed by the careful cleaning of the ZnSe surface by means of a soft polishing with the diamond paste and subsequently with a wet free-of-wood tissue. Other ATR studies of the *in situ* irradiation of glyoxylic acid adsorbed on TiO_2 carried out with both, a diamond-coated ZnSe and a non-coated ZnSe prism (2.7 eV band gap), suitably proved that no significantly different results are obtained concluding that most of the UV light is indeed absorbed by the TiO_2 film [34]. A more detailed discussion concerning this point can be found in Ref. [21].

Sequential spectra of the TiO_2 layer equilibrating with a circulating oxalic acid-free aqueous solution were collected in the dark and under UVA illumination (reference spectra). Each final spec-

trum was the average of 250 scans. The spectra were recorded sequentially without any delay time every 2.15 min and have a spectral resolution of 4 cm^{-1}. The level of noise was always lower than 0.005 absorbance units, approximately 4–5% of the absorbance in the region of interest for this study.

Adsorption measurements in the dark were performed replacing the circulating blank solution by a 2×10^{-3} mol l^{-1} oxalic acid solution. The IR signal amplitudes were allowed to reach stable values using the criteria of assuming equilibrium when there are less than 4% changes (level of noise) in 13 min, the time necessary to collect 6 spectra. This was a compromise between the number of evaluated spectra and the time required for their acquisition, since long equilibrium times can favour further slow processes, e.g. surface reconstructions, responsible for an increase of the TiO_2 adsorption capacity.

The photocatalytic measurements were carried out by illuminating the systems immediately after the adsorption measurements were performed. Sequential spectra were continuously recorded during 5.6 h. The final spectra were always obtained by subtracting the corresponding last reference spectrum (either in the dark or under UV(A) illumination).

For all experiments, 30 ml of circulating solution were employed at a flow rate of approximately 4 ml min^{-1}. Any contributions of dissolved oxalic acid to the FTIR spectra have been found to be negligible at the generally employed concentration of 2×10^{-3} mol l^{-1}. Thus, every detected signal was attributed to adsorbed species at the surfaces of the nanoparticles. The pH of the circulating solution was fixed and carefully kept constant at 3.70 ± 0.02 with a programmed dosing unit. The ionic strength was adjusted to 0.01 mol l^{-1} with KCl and during the entire experiment the solution was constantly purged with O_2.

3. Theoretical procedures

As in our previous studies [1,2] the semiempirical method (MSINDO) [35] modified symmetrically orthogonalized intermediate neglect of differential overlap was the quantum chemical method of choice employed for the theoretical calculations in this work. Surfaces were modelled with the cyclic cluster model (CCM) which is based on a molecular cluster with periodic boundary conditions [36,37]. Different from other solid-state methods currently available, MSINDO-CCM allows excited-state calculations for periodic systems at the configuration interaction (CI) level. Recently, the CI with singles (CIS) method was implemented in MSINDO-CCM [38]. Analytical gradients allow structure optimization of adsorbed molecules on surfaces in the excited state [39]. Specific interactions of the surface with the solvent are taken into account by monolayer adsorption, *vide infra*. Long-range electrostatic solvent effects have been considered by the conductor-like solvent model (COSMO) including excited-state gradients [40]. All two-dimensional cyclic cluster calculations (CCM-2D) were done by relaxing the first surface layer of the cluster using analytical gradients and an updated Hessian procedure. The lattice parameters and the atom positions in the bulk of the cluster were fixed to the values obtained from the previous three-dimensional calculation (CCM-3D) [2]. The (100) and (110) planes for anatase and rutile, respectively, were used as representative surfaces according to respective high resolution transmission electron microscopy (HRTEM) [9] investigations.

In our CIS approach, only *singly excited* configuration functions were employed. Different from ab initio methods where at least implicit doubles corrections (CIS(D)) are necessary, and it has been shown by Zerner et al. [37] that CIS without doubles corrections leads to reasonable excitation energies in semiempirical methods where dynamic electron correlation is accounted for by the empirical parameters. This is similar as for the widely applied TD-DFT method which is technically comparable to CIS, but implicitly contains dynamic correlation in the Kohn–Sham orbital energies. Since the systems studied here are rather complex, the usage of sophisticated methods is not possible. However, by means of our simplistic approach, we succeed in reproducing experimental results on the basis of a quantitative agreement between calculated (with MSINDO-CCM-CIS) and experimentally determined excitation energies for the present system. In fact, the calculated optical band-gap energies of both the free molecules and the TiO_2 surfaces are more than 1 eV above the measured values (4.0 eV for oxalic acid [41], and 3.2 eV for the band gap of anatase [42]). We therefore restrict the present discussion to qualitative aspects of the electronic structure. The CIS method with selected configurations was already applied in an early SINDO1 study of photogenerated ·OH radicals on anatase nanoparticles [43].

In the present study, it was assumed that although excitation into higher states is possible, radiationless relaxation to the lowest excited states is fast. The energetic distances between the low-lying excited states are smaller by 1–2 orders of magnitude as compared to those between the lowest excited state and the ground state; therefore, transitions between the former are assumed to be much faster. Hence, in order to simplify the discussion, MSINDO-CCM-CIS calculations are presented only for the *first* excited *singlet* state (S_1) and the *second* excited *singlet* state (S_2). The corresponding bond-order differences between two atoms i and j in the ground and in the excited state, ΔB_{ij}, for each system were calculated according to Eq. (1):

$$\Delta B_{ij} = B_{ij}^{ex} - B_{ij}^{gr} \tag{1}$$

A negative or a positive ΔB_{ii} value between the excited and ground state of the same atom, represents a loss or a gain, respectively, of electron density on this atom. The electron–hole pair formation in the TiO_2 upon band-gap irradiation (UV(A) illumination) of the systems postulated from experiments is represented by the charge shift of the atoms upon excitation from the ground state. Thus, the involved atoms are assumed to trap the photogenerated hole or electron in the corresponding calculated excited state. A negative or a positive ΔB_{ij} value between two different atoms represents a weakening or a strengthening, respectively, of the corresponding bond. Since B_{ij} values of 1 represent a single bond between atom i and j, and 2 a double bond, values of 0.5 indicate a weakened bond which can be easily broken. For the present systems, ΔB_{ij} values above 0.1 are considered as significant and those above 0.2 as strong. The bond-order changes were used as indication for chemical processes that can be expected in the excited state. For selected cases, we performed explicit geometry optimizations in the excited states with MSINDO-CCM-CIS using the COSMO.

4. Results and discussion

4.1. ATR-FTIR spectra and bulk photocatalysis. Photocatalytic activity of the materials

Fig. 1*a* and *b* shows the comparison of the ATR-FTIR spectra of adsorbed oxalic acid from an aqueous solution on rutile R15 and on anatase S230, respectively, after the first equilibrium in the dark and after the UV(A) illumination period.

Fig. 1*c* and *d* shows the time evolution of the total integrated IR spectral signals of adsorbed oxalic acid from an aqueous solution on rutile R15 and on anatase S230, respectively. Fig. 1*e* and *f* shows the time evolution of integrated spectral area of the five most important bands belonging to adsorbed oxalic acid on rutile R15 [1] and anatase S230 [2], respectively.

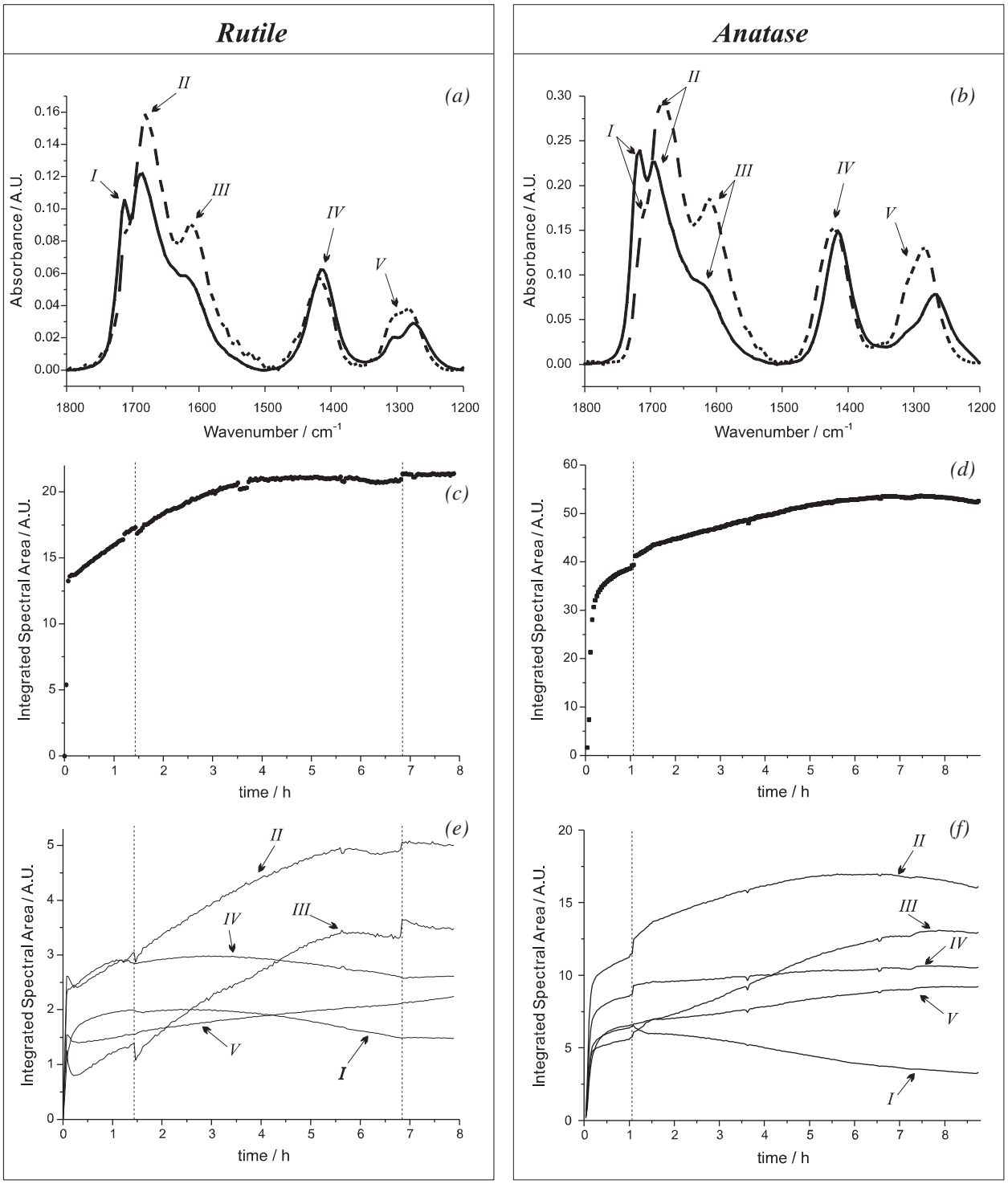

Fig. 1. (*a*) and (*b*) – ATR-FTIR spectra of the adsorbed oxalic acid from an aqueous solution on the rutile (R15) film and on the anatase (S230) film, respectively, after equilibrium in the dark (solid line), after of UV(A) illumination (dotted line). (*c*) and (*d*) – Time evolution of the total integrated IR spectral signals for rutile and anatase, respectively. (*e*) and (*f*) – Time evolution of the integrated spectral area of the most important bands belonging to adsorbed oxalic acid. As the bands are not completely resolved and in some cases they overlap, the integration limits of the bands are both first minima on the right and the left of the maximum of the band: total area: 1800–1200 cm^{-1}; *band I*, 1800–1703 cm^{-1}; *band II*, 1703–1648 cm^{-1}; *band III*, 1648–1509 cm^{-1}; *band IV*, 1509–1351 cm^{-1} and *band V*, 1351–1200 cm^{-1}. (*d*) and (*f*) – Reprinted with permission from Ref. [44]. Copyright 2007 Water Science Technology.

It is obvious that an important increase of the total integrated spectral area is observed in both cases, i.e., for rutile (Fig. 1*c*) as well as for anatase (Fig. 1*d*), upon UV(A) illumination of the systems. This increase is the logical consequence of the fact that an increase of all individual bands is observed (see Fig. 1*e* and *f*), with the exception of band *I* for anatase and bands *I* and *IV* for rutile the intensity of which decreases upon UV(A) illumination. There are, on the other hand, only slight changes in the frequency band positions under UV(A) irradiation. The increase of the total integrated spectral area observed in Fig. 1d has been discussed previously

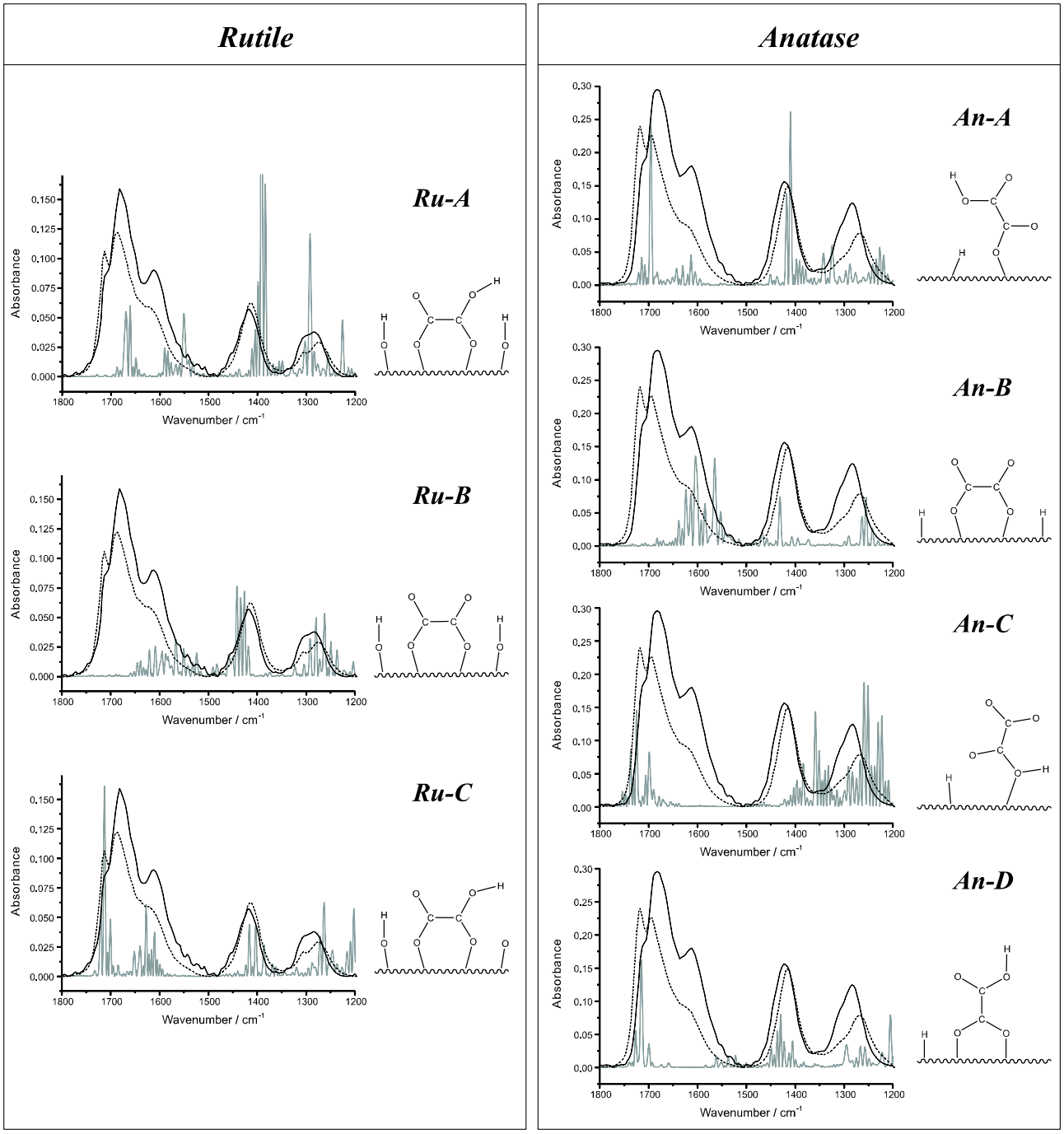

Fig. 2. Experimental ATR-FTIR spectra of adsorbed oxalic acid on rutile R15 (left row) and on anatase S230 (right row) in comparison with the calculated vibration spectra of the corresponding adsorption structures according to Refs. [1] (rutile) and [2] (anatase). Dashed (equilibrium in the dark) and solid black lines (after UV(A) illumination): experimental spectra and grey lines: calculated spectra.

[44] taking into account three different models, (i) the deaggregation of particle agglomerates induced by the action of the thermal energy released upon the recombination of the photogenerated electron–hole pairs [45], (ii) the photogeneration of surface OH groups upon the dissociative water chemisorption on cleaved surface Ti–O bonds [46,47], and (iii) the photodesorption of water molecules coadsorbed at equilibrium conditions with oxalic acid. While (i) and (ii) are suggestions found in the literature, (iii) was a novel mechanism suggested in Ref. [44]. It is a common feature of all three models that new surface sites are freshly exposed upon the action of UV(A) illumination of the systems, hence increasing their oxalic acid adsorption capacity.

Other chemical entities but oxalic acid have been discarded as possibilities of producing the observed spectral changes [22]. Hence, as stated previously, all spectral changes can be attributed to surface reactions/speciation changes of the adsorbed oxalic acid structures.

The changes in the ATR-FTIR band intensities observed during the periods of darkness have been discussed in Ref. [1] for rutile and in Ref. [2] for anatase. In this work, we will therefore focus on the UV(A) illumination data. Fig. 2 shows the comparison of the experimental (dark and UV(A) illumination) and the calculated FTIR spectra. However, it should be noticed that out of the in Refs. [1,2] calculated set of favourable binding structures, the most sta-

ble ones were selected and are denoted here as follows: ***Ru-A***, ***Ru-B*** and ***Ru-C*** are the corresponding identifications for the oxalate complexes on rutile, while ***An-A***, ***An-B***, ***An-C*** and ***An-D*** are those for the complexes on anatase.

The photocatalytic activities of both materials were investigated previously (see Ref. [22] for details and Ref. [2] for the discussion of the adsorbed concentration at equilibrium in the dark as well as for additional adsorption measurements on anatase S230) by measuring the bulk concentration of oxalic acid before and after UV(A) illumination of the systems. While the photocatalytic degradation of oxalate was experimentally verified with anatase S230 being the photocatalyst, it was not possible to confirm this in the case of the rutile R15 system.

Hence, the interpretation of the spectroscopic results, either in the dark or under irradiation, is a delicate task aiming to reveal the complex scenario induced upon the adsorption of oxalic acid on anatase and on rutile surfaces, respectively. The present work should therefore be regarded as a first step to clarify the fundamental mechanisms of the photodegradation and of the photoreactions of these surface complexes. The mechanisms proposed in the next sections are based on the simplified systems of complexes shown in Fig. 2.

4.2. Kinetic behaviour of the adsorbed species upon UV(A)-illumination

Due to the strong infrared absorption of the carbonyl functional group, i.e., one of the most powerful structural probes in infrared spectroscopy, and the fast convergence of the simulated spectral peaks [1,2] in the region 1800–1500 cm^{-1}, only bands *I*, *II* and *III* will be used in the following to draw qualitative conclusions (see Fig. 3).

As derived from Refs. [1,2], for the case of rutile and anatase, respectively, the ATR-FTIR bands are assigned as follows. For rutile (see left row of Fig. 2), band *I* contains contributions from species ***Ru-C***, band *II* from species ***Ru-A*** and band *III* from species ***Ru-B*** and ***Ru-C***; while for anatase (see right row of Fig. 2) band *I* contains contributions from species ***An-C*** and ***An-D***, band *II* mainly from species ***An-A*** with a small contribution from ***An-C*** and band *III* mainly from species ***An-B*** with a small contribution from ***An-A***.

It should be noted here that the division into apparently separate bands used from here on must be taken with care since it is a simplistic attempt to analyse a group of spectra originating from a mixture of adsorbed species at various facets of the nanoparticles. Therefore, in order to make progress for future studies, we simplify this complex scenario: based on our previous combined experimental and theoretical studies, it is assumed that the complexes shown in Fig. 2 suffice to represent the surface coverage of oxalate on both, the anatase (100) and the rutile (110) facets. This simplification does neither consider different facets of both polymorphs nor the adsorption at corners or edges.

The close inspection of Fig. 3*a* demonstrates that after structure ***Ru-C*** reaches its equilibrium in the dark, as indicated by the time evolution of band *I*, its surface concentration slowly decreases under UV(A) illumination. The most stable species ***Ru-A*** and ***Ru-B***, as indicated by bands *II* and *III*, increase their surface concentration until a maximum is reached. Then, a slight decrease of their concentration is observed. It is also observed that immediately after the lamps have been switched on, species ***Ru-A*** and ***Ru-B*** suffer a small decrease in their surface concentration, followed by a continuous increase. Hence, species ***Ru-A*** and ***Ru-B*** are very likely involved in two competing reactions, one being their corresponding photocatalytic degradation, as evinced by a slight decrease in their surface concentration, i.e., during the last hour of UV(A) illumination and also immediately after the illumination was started; while the other is an adsorption reaction on additionally available sites left empty following the photocatalytic degradation of species ***Ru-C***.

As a result, there is an overall increase in the surface concentration of species ***Ru-A*** and ***Ru-B***, with the latter reaction being very likely more important than their photocatalytic degradation. However, a possibility that cannot be excluded is the slow conversion of species ***Ru-C*** into species ***Ru-A*** and/or ***Ru-B*** at the expense of the energy brought to the TiO_2 surface by the light. Otherwise, as stated above, it is photocatalytically degraded opening new surface sites for the additional adsorption of species ***Ru-A*** and ***Ru-B***. Moreover, species ***Ru-A*** and ***Ru-B*** can also adsorb at new active sites left by, for example, the photodesorption of water molecules [44]. It must be mentioned that although the surface rearrangement of species ***Ru-C*** into species ***Ru-A*** and ***Ru-B*** is thermodynamically favoured, it does not occur in the dark [1] while it indeed occurs when additional energy is provided to the system through the UV(A) irradiation. In a subsequent period of darkness, the surface concentrations of all species remain constant, especially in the case of species ***Ru-C***, and in the case of species ***Ru-A*** and ***Ru-B*** after a slight and fast initial decrease.

For anatase, as shown in Fig. 3*b*, the intensity of band *I* decreases under UV(A) illumination while the corresponding intensities of bands *II* and *III* increase. In particular, band *I* decreases, first rapidly right after the lamps are switched on; and later in a slower fashion; bands *II* and *III* increase until they reach a plateau and decrease slowly at the end of the experiment.

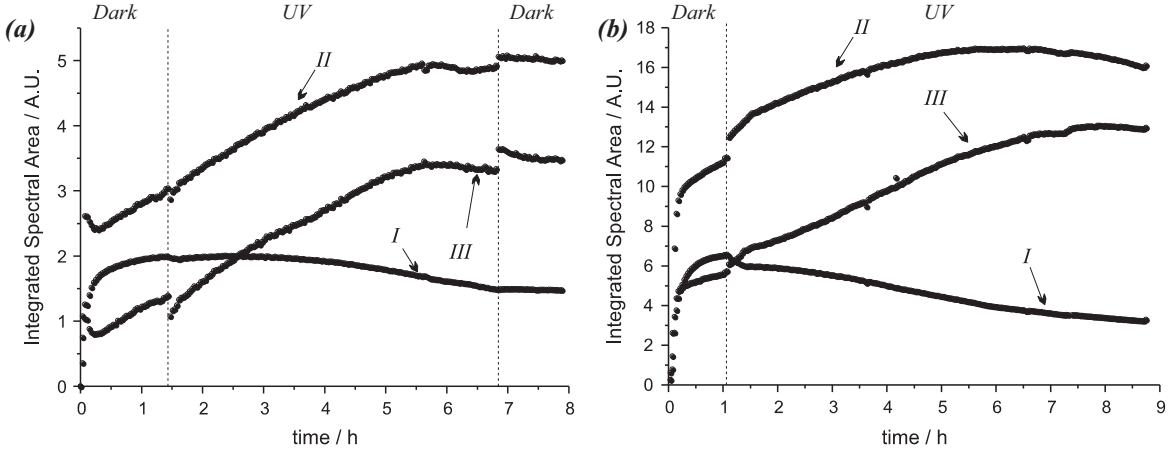

Fig. 3. Integrated spectral area from *bands I*, *II* and *III* as a function of time for the case of (*a*) rutile and (*b*) anatase. The points have been connected with lines for visual clarity (from Fig. 1e and f).

Although the spectral changes are similar to those depicted in the case of rutile (Fig. 3*a*), neither the time evolution of the FTIR bands nor the nature of the adsorbed species involved are exactly the same (see Fig. 2).

Species ***An-C*** and ***An-D***, as indicated by band *I*, decrease in their surface concentration very fast initially and slower afterwards. These species either interconvert to more stable species or are photocatalytically degraded leaving their corresponding active sites for the adsorption of additional oxalic acid molecules. Species ***An-A*** and ***An-B*** populate the surface of anatase, as indicated by bands *II* and *III*. In a manner analogous to the case of rutile, surface rearrangements to more stable or iso-energetic structures are observed under UV(A) irradiation with the surface concentration of species ***An-A*** increasing instantaneously. This increase can be linked to the fast decrease of species ***An-C*** and ***An-D***. The monodentate species ***An-A*** reaches saturation after approximately 4 h of UV(A) illumination followed by a subsequent and slow decrease of its surface concentration. As indicated by band *III*, species ***An-B*** reaches saturation as well, however, later than species ***An-A*** suggesting that species ***An-A*** can undergo direct photocatalytic degradation or rearrange to the bidentate species ***An-B***.

4.3. Configuration interaction calculations: excited-state properties and surface reactions

The electronic properties of the lowest excited singlet states of all systems were studied with MSINDO-CCM-CIS for the 3 surface complexes in the case of rutile (Table 1) and for the 4 surface complexes in the case of anatase (Table 2).

A significant increase of the electron density (photogenerated electron trapping) on the C atoms (in the S_1 state) and the Ti atom where the oxalic acid is bound (S_2) is observed for the most stable species ***Ru-A*** (Table 1). The two O atoms belonging to the adsorbed oxalic acid, O_g and O_d (see structure ***Ru-A*** in Table 1) become more positive both in S_1 and S_2 states, indicating that there is a trapping of the photogenerated hole in the adsorbed molecule in both cases. Thus, the adsorption sites, including the adsorbed oxalic acid and the surface, are apparently involved in the excitation. On the other hand, the bond between the surface Ti site and oxalic acid is not affected, whereas intramolecular bonds are weakened, C_e–O_c, C_e–O_h in S_1 and C_f–O_g in S_2. In particular, if the C_e–O_h bond cleaves, an ·OH radical is released to the bulk solution. As the C–C bond is not affected in S_1 or S_2, no or very little photocatalytic degradation of this species is expected to occur. Thus, these results can be taken as a plausible explanation for the spectral changes shown in Fig. 3*a* (band *II*), where the surface concentration of species ***Ru-A*** increases until it reaches saturation under UV(A) illumination and decreases only slightly upon further irradiation. For this structure, a geometry optimization in the S_1 state was performed. As predicted by the bond orders, the average Ti–O distance did not change significantly (from 2.000 to 2.003 Å). But also the C–O distances only change slightly, from 1.280 to 1.286 Å (C_e–O_c), and from 1.368 to 1.358 Å (C_e–O_h). The main effect is an elongation of the C–C bond, from 1.554 to 1.618 Å. This indicates that (a) bond-order differences do not always reliably predict the geometric changes in the excited states, and (b) photodegradation does not occur within the first fs after light absorption as this is the timescale of the calculated geometry relaxation.

In species ***Ru-B*** (Table 1), the increase of negative charge is on both Ti atoms where the oxalic acid molecule is adsorbed, increasing even more in S_2. The four O atoms which belong to oxalic acid become more positive in S_1, while all the atoms of the adsorbed molecule become more positive in S_2. The photogenerated electron–hole pair is once again trapped at the adsorption sites, i.e. adsorbed oxalate and the TiO_2 surface, respectively, with the electron being mainly localized at a Ti atom and the hole at the adsorbed oxalic acid molecule. Different from species ***Ru-A***, in the case of species ***Ru-B***, the entire adsorbed molecule is oxidized. While bonds between the adsorption Ti site and the oxalate are not affected, the bond between the two surface Ti atoms is weakened, as well as the C–C bond in the molecule in both excitation states. This molecule very likely undergoes photocatalytic degradation into smaller species via the cleavage of the C–C bond. The formation of two adsorbed CO_2 molecules is therefore expected. Both positively charged CO_2 molecules can compensate charges with their corresponding negatively charged Ti surface atoms leaving the surface unchanged. Fig. 4 shows schematically the corresponding reaction. Indeed, geometry optimization on the S_1 energy hypersurface results in even shorter Ti–O and O–C distances, while the C–C bond length is increased from 1.523 to 1.581 Å consistent with a weakening of the bond, thus favouring the dissociation into two CO_2 molecules. However, additional energy uptake from vibrations or collisions with solvent molecules is necessary to actually break the C–C bond which is in accordance with the observed timescale.

The time evolution of *band III* in Fig. 3*a* suggests photocatalytic degradation of species ***Ru-B*** after some hours of UV(A) illumination occurring in a more pronounced manner as compared to species ***Ru-A***. Such experimental observations can be linked to the fact that the surface concentration of species ***Ru-A*** can be increased via a surface reaction, i.e. the protonation of species ***Ru-B*** triggered by the light absorption, and alternatively, according to the analysis of the excited states, via the photocatalytic degradation of species ***Ru-B*** leaving behind new active sites for the further adsorption of additional oxalic acid molecules, e.g., as species ***Ru-A***.

For species ***Ru-B***, the surface Ti–Ti bond can be cleaved in both, the S_1 and the S_2 states. A possible interpretation is that a surface reconstruction mediated by an oxalic acid molecule follows the UV(A) irradiation. Additional O atoms from the chemisorption of dissociated water molecules can bind in between these Ti atoms and new surface OH groups can be thus created. This is in good agreement with experimental observations (obtained in the absence of adsorbed oxalic acid) reported by Hashimoto and coworkers [48] who used the model of photogenerated surface OH groups to explain the superhydrophilic characteristics acquired by TiO_2 surfaces upon UV(A) illumination. In our case, oxalic acid would mediate such a mechanism. Although, to the best of our knowledge, it is still not known from where exactly the ·OH radical originates in a photocatalytic process, i.e. from an irradiated adsorbed water molecule or from an excited adsorbed organic ligand, the presence of ·OH radicals on irradiated titania surfaces has been proven experimentally [49].

The two similar structures ***Ru-C*** that (due to free rotations around the C–C bond) were considered to be the same monodentate species (Table 1), show an increase in the negative charge on both C atoms in S_1, while an increase of electron density in S_2 is observed also on the Ti atom to which the molecule is adsorbed. One or two O atoms from the adsorbed molecule become more positive in S_1 and S_2. The bond between the surface Ti adsorption site and the molecule is not affected by these excitations. Many intramolecular bonds in S_1 between a C and an O atom are weakened, while, on the other hand, the C–C bond is strengthened. The S_1 geometry optimization basically confirms the trends of the bond orders. There are no significant changes in the Ti–O, O–C and C–C bond lengths. The main effect is a change of the molecular orientation and a slight elongation of the C_d–O_f bond, from 1.389 to 1.396 Å.

In the case of the photocatalytic cleavage of the C_d–O_f bond in S_1 (Table 1), species ***Ru-C*** can interconvert to species ***Ru-B*** provided that the neighbouring H atom from the OH group adsorbed to the nearest surface Ti atom is taken by the leaving fragment O_f–H_i of the molecule, thus forming a water molecule. Species ***Ru-B***

Table 1
Rutile – bond-order differences (ΔB) according to MSINDO-CCM-CIS calculations for the first (S_1) and second (S_2) excited singlet state of species ***R-A2***, ***R-A4*** and ***R-C3.*** Negative or positive values on the same atom (ΔB_{ii}) indicate the location of the hole or the electron trapping, respectively. Negative or positive values on different atoms (ΔB_{ij}) indicate the weakening or the strengthening of the bond between those atoms, respectively. A scheme of the molecules is also provided with white or black circles at the atoms which become more negative and more positive, respectively. The sizes of the circles are proportional to the increase or decrease of electron density. Bonds which are weakened due to excitation are drawn as thick dashed grey bonds, while those which strengthened are represented as a thick solid black stripe.

ΔB	***R-A2***				***R-A4***				***R-C3***							
	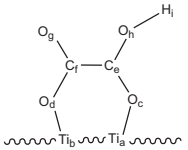				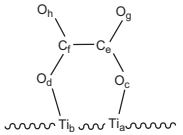				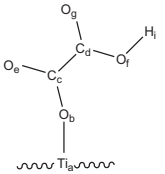				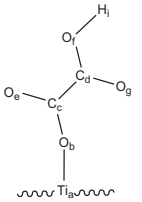			
	S₁		***S₂***		***S₁***		***S₂***		***S₁***		***S₂***		***S₁***		***S₂***	
ΔB_{ii} hole	O_g–O_g O_d–O_d	−0.239 −0.171	O_d–O_d O_g–O_g	−0.165 −0.132	O_g–O_g O_h–O_h O_c–O_c O_d–O_d	−0.164 −0.156 −0.118 −0.118	O_g–O_g O_h–O_h O_d–O_d O_c–O_c C_e–C_e C_f–C_f	−0.178 −0.167 −0.164 −0.158 −0.107 −0.100	O_b–O_b O_e–O_e	−0.126 −0.122	O_e–O_e O_g–O_g	−0.201 −0.177	O_e–O_e	−0.110	O_e–O_e O_g–O_g	−0.179 −0.161
ΔB_{ii} electron	C_e–C_e	0.404	Ti_b–Ti_b C_f–C_f	0.135 0.296	Ti_a–Ti_a Ti_b–Ti_b	0.211 0.247	Ti_a–Ti_a Ti_b–Ti_b	0.321 0.414	C_d–C_d C_c–C_c	0.150 0.184	C_c–C_c Ti_a–Ti_a	0.135 0.248	C_d–C_d C_c–C_c	0.180 0.182	C_c–C_c Ti_a–Ti_a	0.159 0.223
ΔB_{ij} bond weakening	C_e–O_c O_h–C_e	−0.228 −0.227	O_g–C_f	−0.121	Ti_a–Ti_b C_e–C_f O_d–O_c	−0.219 −0.174 −0.164	Ti_a–Ti_b O_d–O_c C_e–C_f	−0.290 −0.124 −0.106	O_f–C_d C_d–O_g	−0.137 −0.123	C_d–C_c	−0.255	O_g–C_d C_d–O_f O_e–C_c	−0.166 −0.144 −0.101	C_d–C_c	−0.311
ΔB_{ij} bond strengthening									C_d–C_c	0.153	O_e–C_c	0.106	C_d–C_c	0.190		
ΔB_{ij} not direct bond	O_g–O_d O_c–O_d O_h–O_d	−0.230 −0.111 −0.105	O_g–O_d O_h–O_g O_h–O_d O_h–C_f	−0.157 −0.139 −0.127 0.144	O_h–O_d O_g–O_c O_g–O_d O_h–O_c O_c–C_f O_d–C_e	−0.135 −0.133 −0.117 −0.116 0.128 0.136	O_h–O_d O_g–O_c	−0.170 −0.165	O_g–C_c O_e–O_b O_g–O_b O_f–O_b O_g–O_e	−0.135 −0.122 −0.109 −0.105 0.151	O_g–O_b O_f–O_b O_e–O_b O_f–O_e H_i–Ti_a C_d–O_b O_f–C_c	−0.170 −0.161 −0.117 −0.102 −0.100 0.170 0.183	O_g–C_c C_d–O_e	−0.180 −0.133	O_g–O_e O_f–O_e O_f–O_b O_e–O_b C_d–O_e O_f–C_c C_d–O_b	−0.260 −0.173 −0.145 −0.108 0.110 0.142 0.173
	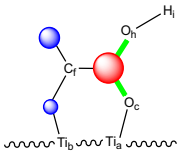		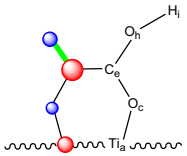		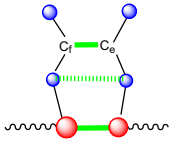		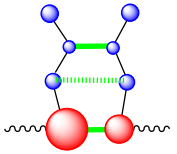		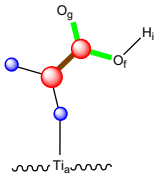		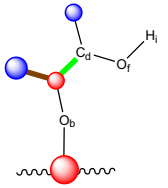		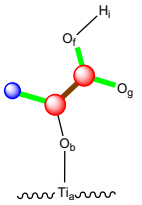		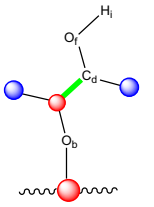	

Table 2

Anatase – bond-order differences (ΔB) according to MSINDO-CCM-CIS calculations for the first (S_1) and second (S_2) excited singlet state of species ***A-C1***, ***A-A3***, ***A-C4*** and ***A-B5***. Ti* represents neighbour Ti atoms in the TiO_2 cluster. Negative or positive values on the same atom (ΔB_{ii}) indicate the location of the hole or the electron trapping, respectively. Negative or positive values on different atoms (ΔB_{ij}) indicate the weakening or the strengthening of the bond between those atoms, respectively. A scheme of the molecules is also provided with white or black circles at the atoms which become more negative and more positive, respectively. The sizes of the circles are proportional to the increase or decrease of electron density. Bonds which are weakened due to excitation are drawn as thick dashed grey bonds, while those which strengthened are represented as a thick solid black stripe.

ΔB	***A-C1***								***A-A3***				***A-C4***				***A-B5***			
	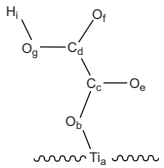				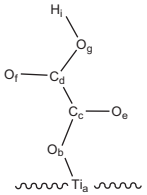				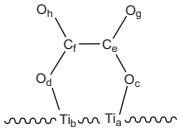				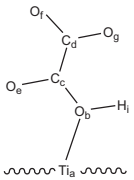				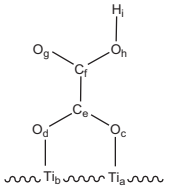			
	S1		***S2***		***S1***		***S2***		***S1***		***S2***		***S1***		***S2***		***S1***		***S2***	
ΔB_{ii} hole	O_e–O_e	−0.226	O_e–O_e O_f–O_f O_b–O_b	−0.150 −0.143 −0.111	O_e–O_e O_b–O_b	−0.123 −0.115	O_e–O_e O_f–O_f	−0.187 −0.159	O_h–O_h O_g–O_g O_c–O_c O_d–O_d	−0.164 −0.164 −0.130 −0.129	O_h–O_h O_g–O_g O_d–O_d O_c–O_c	−0.168 −0.168 −0.163 −0.163	O_g–O_g O_f–O_f	−0.138 −0.105	C_c–C_c O_f–O_f O_g–O_g O_e–O_e O_b–O_b	−0.261 −0.183 −0.179 −0.137 −0.137	O_c–O_c	−0.106	O_d–O_d	−0.102
ΔB_{ii} electron	Ti_a–Ti_a C_d–C_d	0.195 0.221	C_c–C_c C_d–C_d	0.140 0.147	C_c–C_c C_d–C_d	0.168 0.193	C_c–C_c Ti_a–-Ti_a	0.165 0.221	Ti_a–Ti_a Ti_b–Ti_b	0.280 0.285	Ti_a–Ti_a Ti_b–Ti_b	0.373 0.374	C_d–C_d Ti_a–Ti_a	0.146 0.239	Ti_a–Ti_a	0.734	C_f–C_f C_e–C_e	0.166 0.170	C_f–C_f C_e–C_e	0.158 0.191
ΔB_{ij} bond weakening	C_d–O_f C_d–O_g	−0.146 −0.136	C_c–C_d C_d–O_g	−0.206 −0.139	O_f–C_d C_d–O_g	−0.166 −0.150	C_c–C_d	−0.271	Ti_a–Ti_b O_c–O_d C_e–C_f	−0.223 −0.164 −0.150	Ti_a–Ti_b O_c–O_d	−0.282 −0.133					O_h–C_f	−0.132	O_h–C_f O_g–C_f	−0.126 −0.100
ΔB_{ij} bond strengthening			C_c–O_g	0.243	C_c–C_d	0.182	C_c–O_e	0.108												
ΔB_{ij} not direct bond	O_b–O_e O_b–O_g O_b–O_f O_b–C_d	−0.162 −0.143 −0.135 0.181	O_e–O_g O_b–O_g O_b–O_e O_b–C_d	−0.209 −0.145 −0.118 0.108	C_c–O_f O_e–C_d O_b–O_e O_f–O_e	−0.170 −0.118 −0.105 0.184	O_b–O_f O_b–O_g O_b–O_e Ti_a–H_i O_e–C_d O_b–C_d C_c–O_g	−0.172 −0.160 −0.118 −0.112 0.103 0.192 0.198	O_d–O_h O_c–O_g O_c–C_f O_d–C_e	−0.147 −0.147 0.132 0.133	O_d–O_h O_c–O_g	−0.167 −0.167	O_b–O_g O_f–O_b O_f–O_g O_b–C_d	−0.174 −0.149 −0.116 0.165	O_f–O_g O_b–O_g Ti^*–Ti_a Ti_a–Ti^* O_f–O_b Ti_a–Ti^* Ti^*–Ti_a	−0.181 −0.132 −0.129 −0.124 −0.114 −0.110 −0.104	O_h–O_d O_d–O_c O_h–O_c O_h–C_e	−0.167 −0.123 −0.121 0.141	O_h–O_c O_d–O_c O_h–O_d O_h–C_e	−0.158 −0.123 −0.120 0.132
	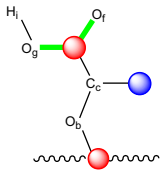		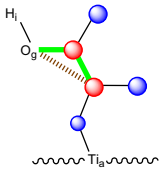		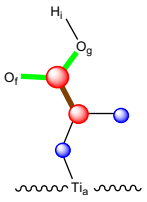		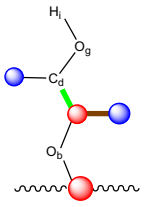		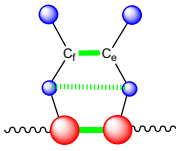		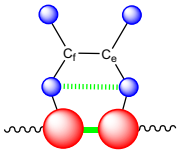		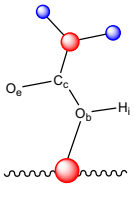		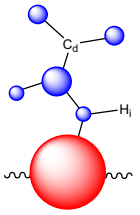		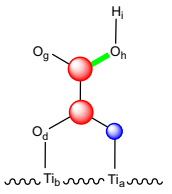		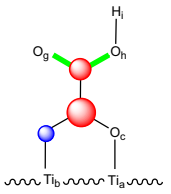	

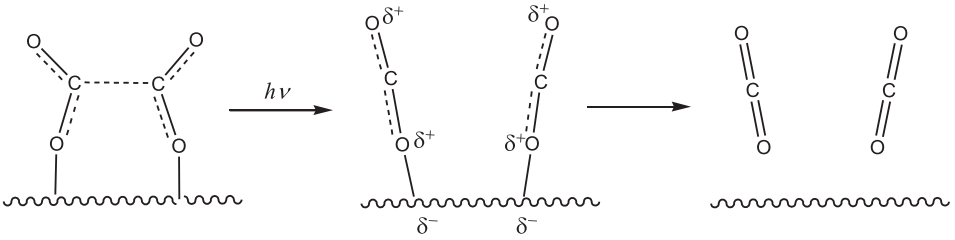

Fig. 4. Possible photocatalytic degradation of species ***Ru-B***.

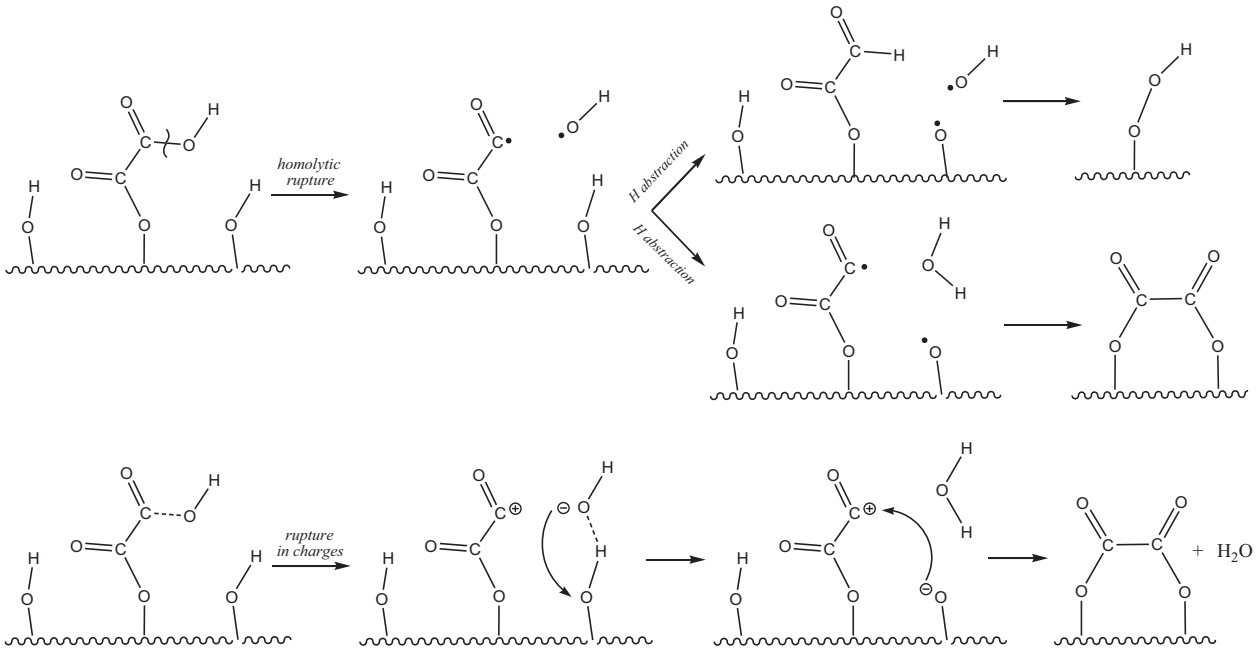

Fig. 5. Possible surface rearrangement of species ***Ru-C*** into ***Ru-B***.

is built when atom C_d binds to the remaining O atom directly bound to the nearest surface Ti atom which had lost its H atom due to the formation of the water molecule. In this case, through the reduction of the C atom, there is an oxidation of the OH group at the same molecule. This reaction can occur via a homolytic cleavage of the C–O bond or via a scission in separated charges. Both possibilities are schematically shown in Fig. 5.

As commented in the previous section, a photocatalytic surface rearrangement of species ***Ru-C*** into structures ***Ru-B*** or ***Ru-A*** suggested from the time evolution of *bands I*, *II* and *III* in Fig. 3*a*, can be explained as an interconversion to species ***Ru-A*** indirectly via species ***Ru-B***. An adsorbed peroxide and an aldehyde molecule, accounting for the oxidation of the OH group and for the reduction of the carboxylic group, respectively, may also be formed in the rearrangement reaction, although neither of both species have been detected experimentally.

According to the ΔB_{CC} value for both ***Ru-C*** structures, the C–C bond breaks in S_2. In this case, the formation of CO_2 is expected in S_2, as also supported by the strengthening of the molecular O_e–C_c bond. One or two CO_2 molecules are the result of the photocatalytic fragmentation of species ***Ru-C*** irrespective of the bond scission (homolytic or into separated charges, see Fig. 6). In addition, adsorbed formic acid is expected to be formed in either of both mechanisms. Since the presence of adsorbed formic acid was not confirmed experimentally [22], degradation via the formation of CO_2 seems to be the most plausible reaction. However, formation of adsorbed formic acid cannot be completely ruled out. In this case, it must be formed in negligible amounts below the detection limit of the analytical method.

The most stable species formed at the anatase (1 0 0) surface, i.e. ***An-A***, was calculated in its two configurations ***A-C1*** and ***A-C2*** (see Ref. [2]) that will be indistinguishable at room temperature due to the free rotation around the C–C bond. In this case, the increase in the negative charge is observed either on only one C atom, C_d, and on the surface Ti atom in S_1; or on both C atoms in S_2 (see Table 2). Hence, the photogenerated electron will be trapped there. One, two or three O atoms of the adsorbed molecule become more positive in S_1 and S_2, with these atoms being the traps for the photogenerated hole in both excitations. As for the case of rutile, the adsorption sites in anatase which include the surface and the oxalic acid molecule appear to concentrate the photogenerated charge carriers upon UV(A) excitation. Two intramolecular bonds in S_1 are weakened, i.e. C_d–O_f and C_d–O_g, while the C–C bond is partially strengthened. The S_1 geometry optimization results in no significant bond length changes. Only the molecular orientation is changed. In a similar manner as for the monodentate species ***Ru-C*** on rutile, by means of the cleavage of the C_d–O_g bond, species ***An-A*** may undergo surface interconversion to the non-protonated bidentate species ***An-B*** analogous to species ***Ru-B*** on rutile (see Fig. 5 for the mechanism). Although this reaction is not thermodynamically favoured in the dark (***An-A*** enthalpy is lower than that of ***An-B***) [2], it can be possible at higher energetic states of the system formed, i.e., under UV(A) illumination. The present MSINDO-CCM-CIS calculations thus provide a possible explanation to interpret the

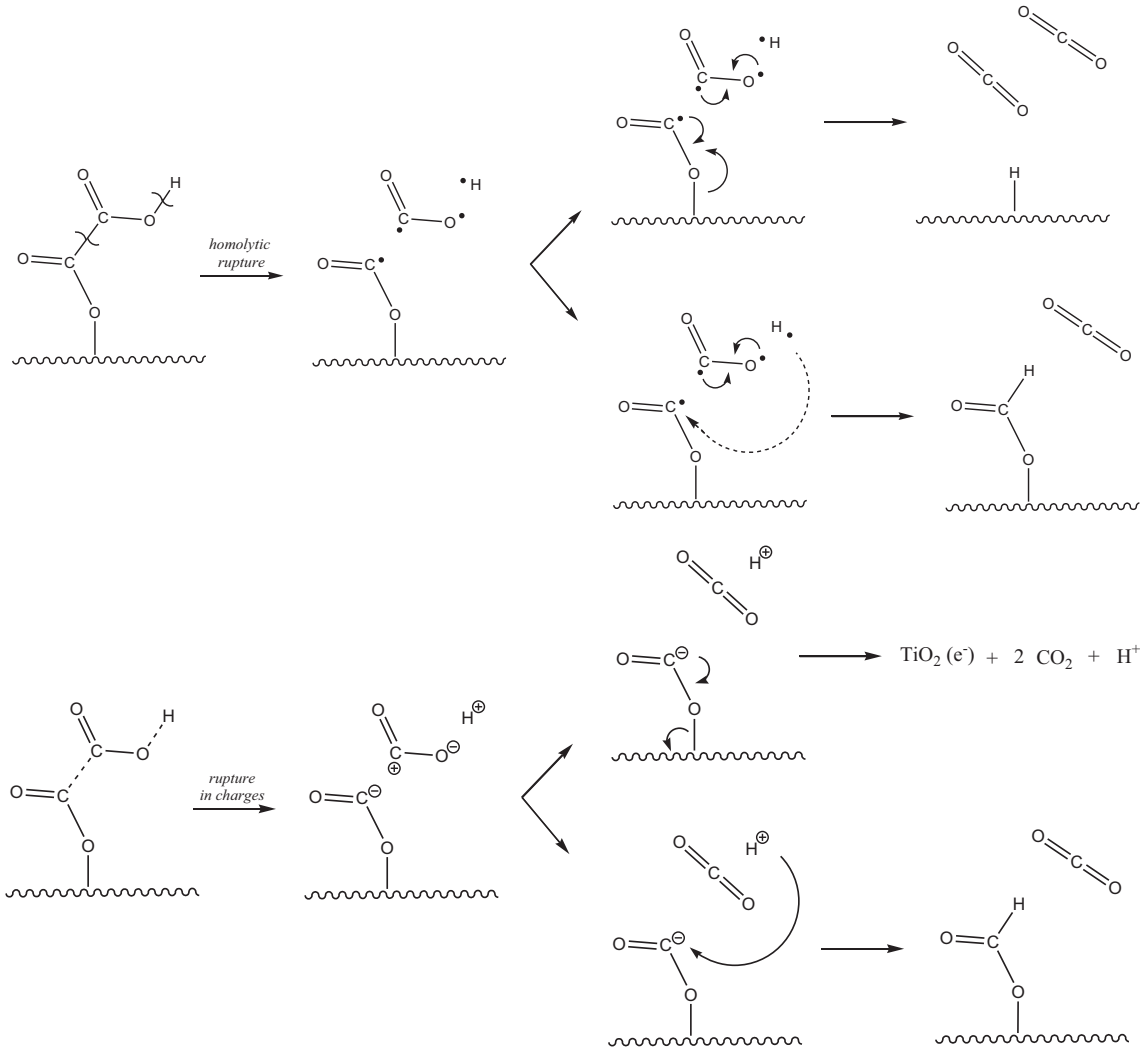

Fig. 6. Possible photocatalytic fragmentation of species ***Ru-C***.

experimental results shown in Fig. 3*b* in which the intensity of the spectral band *II* associated to species ***An-A*** decreases after 5 h of UV(A) irradiation, while at the same time, the intensity of spectral band *III* associated to species ***An-B*** increases and reaches saturation. An additional reason for a decrease in the surface concentration of species ***An-A*** is its direct photocatalytic degradation as mentioned in the previous section. The analysis of the S_2 excitation of species ***An-A*** supports this hypothesis yielding the following mechanism. The C–C bond cleavage occurs together with the strengthening of the C_c–O_e and the C_c–O_g bond, resulting in the formation of adsorbed bi-carbonate and a CO molecule. Fig. 7 shows this reaction schematically.

Bi-carbonate has not been detected experimentally as a major intermediate [22] indicating that as in the case of formic acid only very small amounts below the detection limit of the employed analytical methods may be formed. An alternative possibility is that bi-carbonate is released very rapidly to the bulk solution and leaves the system as CO_2 due to the low bulk pH. Formation of CO cannot be completely ruled out since it was observed in other studies during the thermal decomposition of aqueous solutions of oxalic acid [50,51] and as a product in the photolysis of gaseous oxalic acid [52]. In our case, CO formation only originates from one particular surface species, ***An-A***, and the total amount formed in the system is expected to be low.

In both excitations of species ***An-A***, S_1 and S_2, the formation of free ·OH radicals is also predicted via the cleavage of the C_d–O_g bond (Table 2).

The bidentate species ***An-B*** (Table 2) appears to yield the same results as the analogous structure on rutile, ***Ru-B***. S_1 and S_2 excitations show very similar results. The increase of the negative charge occurs on both Ti atoms where the oxalic acid molecule is adsorbed, while the four O atoms of the molecule become more positive. For this species, the photogenerated electron is trapped in the TiO_2 surface while the counterpart (the hole) is localized within the oxalic acid molecule. Bonds between the adsorption Ti site and the oxalic acid are not affected, whereas the C–C bond in the molecule is weakened. This species can undergo photocatalytic degradation yielding two adsorbed CO_2 molecules in a similar reaction as for ***Ru-B*** on rutile (Fig. 4). This is also indicated by the calculated C–C bond length change in the S_1 state, i.e. +0.03 Å.

In the S_1 excitation of species ***An-C*** (Table 2), there is an increase in the negative charge on one C atom, C_d, and in the binding Ti surface atom, while in the S_2 excitation, the increase in the negative charge is extreme and only on the Ti atom. In S_1, two O atoms become more positive indicating that there is a hole trap on these atoms. In S_2, almost all atoms in the adsorbed molecule with the exception of one C atom become more positive. For species ***An-C,*** the calculations suggest that the hole trapping occurs

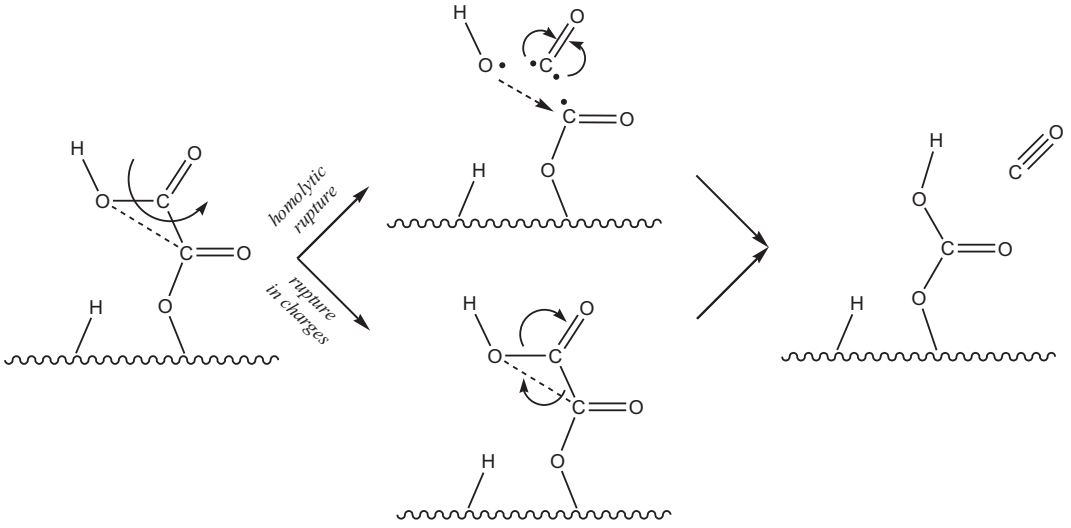

Fig. 7. Possible photocatalytic degradation of species ***An-A***.

entirely on the molecule, suggesting that this species acts as an efficient electron and hole trap. Consequently, this structure should be a good recombination centre.

As neither intramolecular nor the surface Ti-oxalic-acid bonds are weakened, species ***An-C*** is not expected to undergo photocatalytic degradation in both, the S_1 and the S_2 excitation. The decrease of the spectral band *I* associated to species ***An-C*** (see Fig. 3*b*) indicates that this species decreases its surface concentration upon UV(A) -illumination. A possible explanation can be that the energy provided by the light increases the instability of species ***An-C*** that can thus desorb and be readsorbed as another more stable species

In species ***An-D*** (Table 2), an increase in the negative charge in both C atoms of the adsorbed molecule is observed in S_1 and S_2, thus assuming that the photogenerated electron will be trapped there. On the contrary, both in S_1 and S_2, there is a hole trapping on the molecule, indicated by the O atom near the TiO_2 surface which becomes more positive. One or two intramolecular bonds are weakened in the excitation, i.e. C_f–O_h and C_f–O_g. Species ***An-D*** can undergo photocatalytic degradation in the S_1 and in the S_2 excitation, but the C–C bond very probably may be cleaved in higher excitation states (not calculated). The decrease of the spectral band *I* associated to species ***An-D*** (Fig. 3*b*) indicates that this species decreases its surface concentration under UV(A) illumination. In this case, as assumed for species ***An-C,*** the energy provided by the light very likely increases its instability and a mechanism of desorption–readsorption into other more stable species can be initiated.

5. Conclusions

Reaction mechanisms of adsorbed oxalic acid occurring under UV(A) illumination and involving the surfaces of TiO_2 as an active reactant have been suggested on the basis of experimental evidence and quantum chemical calculations. The three most stable surface complexes on rutile (110): ***Ru-A***, ***Ru-B*** (two bidentate structures) and ***Ru-C*** (one monodentate structure) and the four most stable ones on anatase (100): ***An-A***, ***An-C*** (two monodentate structures), ***An-B*** and ***An-D*** (two bidentate structures) that have been identified previously (Refs. [1,2]) to be representative of the surface speciation under dark equilibrium conditions were found to participate in different chemical reactions, showing different photoreactivities towards UV(A) light excitation.

Under UV(A) illumination, the concentration of the species ***Ru-C*** decreases, while those of species ***Ru-A*** and ***Ru-B*** increase. Species ***Ru-A*** undergoes photocatalytic degradation releasing an ·OH radical, while species ***Ru-B*** converts into two CO_2 molecules. The photoreactions of species ***Ru-C*** are found to be: (i) interconversion to the bidentate species ***Ru-A*** with the elimination of a water molecule and (ii) reduction to an aldehyde form with the oxidation of a neighbouring adsorbed OH group into an adsorbed ·OOH radical and (iii) the direct conversion into one or two CO_2 molecules. Adsorbed formic acid may also be produced during the last reaction.

For the case of anatase under UV(A) illumination, the surface concentrations of ***An-C*** and ***An-D*** decrease while those of ***An-A*** and ***An-B*** increase. We found that species ***An-A*** can (i) be converted to species ***An-B*** releasing an ·OH radical or a water molecule, (ii) be reduced to an aldehyde form with the oxidation of the nearby surface OH to adsorbed ·OOH, (iii) undergo photocatalytic degradation releasing one or two CO_2 molecules and eventually adsorbed formic acid, or (iv) convert to adsorbed bicarbonate with the elimination of CO. Species ***An-C*** is not found to undergo photocatalytic degradation, but it appears to act as a very efficient electron–hole trap and thus a recombination centre. Species ***An-B*** is found to undergo easily photocatalytic degradation yielding two CO_2 molecules. Species ***An-D*** undergoes direct photocatalytic degradation releasing ·OH radicals and as it is the only species forming a five-membered ring, it is assumed to be highly preferred for further radical attack.

Direct oxidation/reduction of oxalic acid at the TiO_2 surface is possible by the hole–electron pairs formed upon UV(A) light absorption and is suggested to occur as the main photocatalytic reaction accounting for its photocatalytic degradation. Radical attack cannot be ruled out, however, on the basis of our results, it is assumed to occur only as a secondary process. In this case, the ·OH radicals involved in the reactions only arise from the cleavage of chemical bonds of the adsorbed oxalic acid molecules and not from the water molecules chemisorbed at the TiO_2 surface.

Thus, the adsorption sites involved in the excitation only include the Ti atoms from the surface and the adsorbate molecule. These results may be a key for the understanding of the different photoreactivities found so far for different organic adsorbates at the TiO_2 surface. In particular, those molecules that are involved in the harvesting of the absorbed energy and/or have the possibil-

ity of producing ·OH radicals can be expected to degrade preferentially by the action of this surface photocatalysis.

Acknowledgments

We gratefully acknowledge the financial support by Agencia Nacional de Promoción Científica y Tecnológica (ANPCYT), Argentina (project PICT-2683); and by Millennium Inorganic Chemicals (now CRISTAL GLOBAL). We want to thank MINCyT (Argentina) and BMBF (Germany) for the financial support of the exchange project AL1209. CBM is a member of the research staff of CONICET. JS gratefully acknowledges financial support from the German Ministry of Science and Technology (BMBF), Grant Number 033RC1012C (Neue Katalysatoren und Technologien für die solarchemische Wasserstofferzeugung, HyCats). TB gratefully acknowledges the financial support by Deutsche Forschungsgemeinschaft within the Collaborate Research Center SFB 813 Chemistry at Spin Centers.

References

[1] C.B. Mendive, T. Bredow, A. Feldhoff, M. Blesa, D. Bahnemann, PCCP 10 (14) (2008) 1960.
[2] C.B. Mendive, T. Bredow, A. Feldhoff, M.A. Blesa, D. Bahnemann, PCCP 11 (11) (2009) 1794.
[3] M.K. Nowotny, J. Nowotny, Solid State Chemistry and Photocatalysis of Titanium Dioxide, Trans Tech Publications LTD, Stafa-Zuerich, 2010.
[4] L.E. Brus, J. Chem. Phys. 80 (9) (1984) 4403.
[5] L.E. Brus, J. Chem. Phys. 79 (11) (1983) 5566.
[6] V.H. Grassian, J. Phys. Chem. C 112 (47) (2008) 18303.
[7] A.Y. Ahmed, T.A. Kandiel, T. Oekermann, D. Bahnemann, J. Phys. Chem. Lett. 2 (19) (2011) 2461.
[8] A.Y. Ahmed, T. Oekermann, P. Lindner, D. Bahnemann, PCCP 14 (8) (2012) 2774.
[9] A. Feldhoff, C. Mendive, T. Bredow, D. Bahnemann, ChemPhysChem 8 (6) (2007) 805.
[10] A. Fujishima, X. Zhang, D.A. Tryk, Surf. Sci. Rep. 63 (12) (2008) 515.
[11] L.J. Liu, H.L. Zhao, J.M. Andino, Y. Li, Acs Catal. 2 (8) (2012) 1817.
[12] D.H. Chen, R.A. Caruso, Adv. Funct. Mater. 23 (11) (2013) 1356.
[13] G. Liu, H.G. Yang, J. Pan, Y.Q. Yang, G.Q. Lu, H.-M. Cheng, Chem. Rev. (2014).
[14] M. Andersson, A. Kiselev, L. Osterlund, A.E.C. Palmqvist, J. Phys. Chem. C 111 (18) (2007) 6789.
[15] H. Kisch, Angew. Chem. Int. Ed. 52 (3) (2013) 812.
[16] P.K.J. Robertson, D. Bahnemann, J.M.C. Robertson, F.W. Hdb, Environ. Chem. 2 (Part M) (2005) 367.
[17] P.K.J. Robertson, J.M.C. Robertson, D.W. Bahnemann, J. Hazard. Mater. 211 (2012) 161.
[18] I. Dolamic, T. Burgi, J. Phys. Chem. B 110 (30) (2006) 14898.
[19] I. Dolamic, T. Burgi, J. Catal. 248 (2) (2007) 268.
[20] I. Dolamic, T. Burgi, J. Phys. Chem. C 115 (5) (2011) 2228.
[21] C.B. Mendive, D.W. Bahnemann, M.A. Blesa, Catal. Today 101 (3–4) (2005) 237.
[22] C.B. Mendive, T. Bredow, M.A. Blesa, D.W. Bahnemann, PCCP 8 (27) (2006) 3232.
[23] U. Diebold, Surf. Sci. Rep. 48 (5–8) (2003) 53.
[24] A.G. Thomas, K.L. Syres, Chem. Soc. Rev. 41 (11) (2012) 4207.
[25] A. Fahmi, C. Minot, P. Fourre, P. Nortier, Surf. Sci. 343 (3) (1995) 261.
[26] B. Hammer, S. Wendt, F. Besenbacher, Top. Catal. 53 (5–6) (2010) 423.
[27] C.H. Sun, L.M. Liu, A. Selloni, G.Q. Lu, S.C. Smith, J. Mater. Chem. 20 (46) (2010) 10319.
[28] C.L. Pang, R. Lindsay, G. Thornton, Chem. Rev. 113 (6) (2013) 3887.
[29] C.T. Campbell, J.R.V. Sellers, Chem. Rev. 113 (6) (2013) 4106.
[30] Z. Dohnalek, I. Lyubinetsky, R. Rousseau, Prog. Surf. Sci. 85 (5–8) (2010) 161.
[31] M.H. Du, J. Feng, S.B. Zhang, Phys. Rev. Lett. 98 (6) (2007).
[32] A.S. Barnard, L.A. Curtiss, Nano Lett. 5 (7) (2005) 1261.
[33] D.G. Gong, V.P. Subramaniam, J.G. Highfield, Y.X. Tang, Y.K. Lai, Z. Chen, Acs Catal. 1 (8) (2011) 864.
[34] G.N. Ekstrom, A.J. McQuillan, J. Phys. Chem. B 103 (48) (1999) 10562.
[35] T. Bredow, K. Jug, Theor. Chem. Acc. 113 (1) (2005) 1.
[36] T. Bredow, G. Geudtner, K. Jug, J. Comput. Chem. 22 (8) (2001) 861.
[37] M.C. Zerner, G.H. Loew, R.F. Kirchner, U.T. Muellerwesterhoff, J. Am. Chem. Soc. 102 (2) (1980) 589.
[38] I. Gadaczek, K.J. Hintze, T. Bredow, PCCP 14 (2) (2012) 741.
[39] I. Gadaczek, K. Krause, K.J. Hintze, T. Bredow, J. Chem. Theory Comput. 8 (3) (2012) 986.
[40] K. Krause, T. Bredow, J. Comput. Chem. 35 (7) (2014) 553.
[41] R.A. Back, Can. J. Chem. 62 (8) (1984) 1414.
[42] L. Chiodo, J.M. Garcia-Lastra, A. Iacomino, S. Ossicini, J. Zhao, H. Petek, A. Rubio, Phys. Rev. B 82 (4) (2010).
[43] T. Bredow, K. Jug, J. Phys. Chem. 99 (1) (1995) 285.
[44] C.B. Mendive, M.A. Blesa, D. Bahnemann, Water Sci. Technol. 55 (12) (2007) 139.
[45] C.B. Mendive, D. Hansmann, T. Bredow, D. Bahnemann, J. Phys. Chem. C 115 (40) (2011) 19676.
[46] R. Pagel, J.K. Dohrmann, J. Phys. Chem. C 111 (11) (2007) 4458.
[47] K. Stopper, J.K. Dohrmann, Z. Phys. Chem. 214 (2000) 555.
[48] N. Sakai, A. Fujishima, T. Watanabe, K. Hashimoto, J. Phys. Chem. B 107 (4) (2003) 1028.
[49] T. Hirakawa, K. Yawata, Y. Nosaka, Appl. Catal. A: Gen. 325 (1) (2007) 105.
[50] A. Dinglinger, E. Schroer, Z. Phys. Chem. A 179 (1937) 401.
[51] L.W. Clark, J. Phys. Chem. 61 (5) (1957) 699.
[52] S. Yamamoto, R.A. Back, J. Phys. Chem. 89 (4) (1985) 622.